

---

# HOW TO BUILD LOW-COST NETWORKS FOR LARGE LANGUAGE MODELS (WITHOUT SACRIFICING PERFORMANCE)?

---

Weiyang Wang<sup>1</sup> Manya Ghobadi<sup>1</sup> Kayvon Shakeri<sup>2</sup> Ying Zhang<sup>2</sup> Naader Hasani<sup>2</sup>

## ABSTRACT

This paper challenges the well-established paradigm for building any-to-any networks for training Large Language Models (LLMs). We show that LLMs exhibit a unique communication pattern where only small groups of GPUs require high-bandwidth communication to achieve near-optimal training performance. Across these groups of GPUs, the communication is insignificant and homogeneous. We propose a new network architecture that resembles the communication requirement of LLMs. Our architecture partitions the cluster into sets of GPUs interconnected with non-blocking any-to-any high-bandwidth interconnects that we call HB domains. Across the HB domains, the network only connects GPUs with non-zero communication demands. We develop an analytical formulation of the training iteration time to evaluate our proposal. Our formulation closely estimates the hardware floating-point utilization within 0.15% from the ground truth established in prior studies for larger models. We show that our proposed architecture reduces the network cost by 37% to 75% compared to the state-of-the-art any-to-any Clos networks without compromising the performance of LLM training.

## 1 INTRODUCTION

LLMs are among the largest and most computationally intensive Deep Neural Networks (DNNs). The latest GPT4 model is estimated to have trillions of parameters and take months to train (OpenAI, 2023b; The-Decoder, 2023). Conventionally, researchers seek to enhance the performance of distributed DNN training and inference through optimizing parallelization strategies (Jia et al., 2019; Zheng et al., 2022; Unger et al., 2022; Wang et al., 2019), sophisticated scheduling (Zhao et al., 2022b; Xiao et al., 2018; Gu et al., 2019), advanced compression (Bai et al., 2021), and even the reconfiguration of the network topology itself (Khani et al., 2021; Wang et al., 2023a; Zhao et al., 2022a). Despite these efforts, LLMs still require significant raw computing power. The GPT3 model from 2020 already requires 355 GPU-years on Nvidia’s V100 GPUs (Brown et al., 2020; Labs, 2020). As Moore’s law slows down, the growth rate of LLM size and computation requirement exceeds the advancement of accelerators, making hyper-scale GPU clusters inevitable. Our conversations with lead machine learning architects in the industry indicate that the next-generation LLMs likely require over 30,000 GPUs of computing power to finish training within a reasonable time. At the same time, scaling the cluster to 32,000 GPUs also allows LLM designers to train smaller models like LLaMa-65B (Touvron et al., 2023) within a day (Meta, 2023), expediting future development.

A GPU-centric cluster typically employs two types of interconnection domains (Nvidia, 2023a). First, a high-bandwidth domain where a few GPUs (e.g., eight for a DGX H100 server) are interconnected with high bandwidth, but short-range communication links like NVLinks (Nvidia, 2023d). We refer to this type of interconnection as the HB domain. The second interconnection domain forms a network capable of any-to-any GPU communication using RDMA-capable NICs, connected in a Clos network architecture. The cluster uses the RDMA protocol on this network to benefit from bypassing CPU and OS entirely through GPU-Direct (Shainer et al., 2011; Nvidia, 2023c).

However, scaling up RDMA networks to tens of thousands of GPUs is challenging. Previous work demonstrated that large-scale RDMA networks are prone to deadlocking and PFC storms (Guo et al., 2016; Bai et al., 2023; Schneider et al., 2016; Goyal et al., 2022; Hu et al., 2016), degrading the performance. Furthermore, as the scale increases, Clos architectures become prohibitively costly (Wang et al., 2023a). Datacenter providers resort to over-subscription to tame costs, worsening the deadlocking problems. Prior work proposed several techniques to enable large-scale RDMA networks and reduce their cost (Zhu et al., 2015; Bai et al., 2023; Wang et al., 2023b; Mittal et al., 2018). These approaches fundamentally depend on the assumption that the network is capable of any-to-any communication. This assumption forms the bedrock upon which datacenters have been conceptualized and developed for several decades.

In this paper, we challenge this assumption and show that

---

<sup>1</sup>MIT CSAIL <sup>2</sup>Meta.

LLM training traffic *does not* require any-to-any connectivity across all GPUs in the network. This paper makes three primary contributions. First, we analyze the traffic pattern of training dense LLMs (§3). We demonstrate that with an optimal parallelization strategy, an LLM training workload requires high-bandwidth any-to-any connectivity *only within discrete subsets of GPUs*, and each subset fits within an HB domain. Across the HB domains, communication only occurs between a few GPU pairs with the same rank in their respective HB domains, and the traffic volume is insignificant. As a result, the conventional any-to-any approach for building datacenter networks adds unnecessary complexity and cost for distributed LLM training.

Motivated by the above observations, we propose a low-cost, high-efficiency network architecture that accurately reflects LLM communication requirements that we name “rail-only” (§4). In our architecture, a cluster is partitioned into multiple HB domains, similar to conventional Clos architectures. Across the HB domains, however, instead of forming a Clos to support any-to-any communication, the network only connects sets of GPUs with non-zero network traffic. Compared to the state-of-the-art Clos design, our network architecture removes the network equipment that does not carry traffic and achieves the same performance as a Clos network. We also examine our design’s fault-tolerance properties and provide recovery methods from failure cases.

Finally, we derive an analytical formula for accurately estimating the training iteration time of LLMs (§5). This formulation provides insights into the training performance of our network design with different LLM parallelization strategies. Unlike previous approaches (Narayanan et al., 2021), our formulation explicitly considers both the computation and communication time, given the LLM hyperparameters, the parallelization strategy, and the training infrastructure. We compare our formulation to published results to validate its accuracy and show that for LLMs with over one trillion parameters, our formulation estimates the training iteration time within 0.15% of the ground truth in hardware FLOP utilization (§6.1).

We evaluate the performance of a rail-only network architecture using our analytical formulation and provide insights into the performance impact of different network and training parameters. Our evaluation indicates that an HB domain of size 256 provides near-optimal performance, within 8.9% of the optimal training iteration time compared to the ideal case where all GPUs reside in a monolithic HB domain. We also show that surprisingly small LLMs exhibit more network overhead than larger ones and demand more network optimization. We discuss the reasons behind this counter-intuitive result (§6.2). In addition, we compare the cost of our proposal (§6.5) to a full-bisection bandwidth any-to-any Clos cluster that achieves the same performance

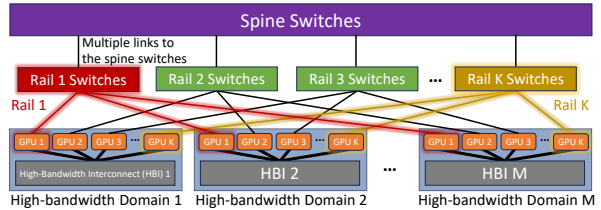


Figure 1. State-of-the-art GPU clusters are based on rail-optimized, any-to-any Clos networks (Nvidia, 2023a).

and show that our LLM-centric network architecture reduces the network cost by 37% to 75%.

## 2 BACKGROUND

In this section, we first introduce the architecture of a conventional GPU-centric cluster. Afterward, we document the predominant parallelization strategies for training LLMs to lay down the foundation of our system design and modeling.

### 2.1 State-of-the-Art GPU cluster Design

The rise of network-heavy ML workloads led to the dominance of GPU-centric clusters, where *individual* GPUs have dedicated NICs (Mudigere et al., 2022). Figure 1 illustrates the network architecture of a typical GPU cluster. Each GPU has two communication interfaces: (i) A local interface to support high-bandwidth but short-range interconnection and (ii) a conventional RDMA-enabled NIC. The local interface connects  $K$  GPUs to provide terabits of non-blocking any-to-any bandwidth in/out per GPU (900 GB/s or 7.2 Tbps for fourth-gen NVLink, for instance). This group of GPUs with fast interconnect forms a *high-bandwidth domain (HB domain)*. Traditionally, HB domains were restricted to a single server (e.g., DGX servers with  $K = 8$  or 16 GPUs). Recently, Nvidia announced the GH200 supercomputer interconnecting  $K = 256$  Grace Hopper Superchips to form one HB domain across multiple racks (Nvidia, 2023b).

To scale training an LLM beyond a single HB domain, GPU cluster operators use RDMA-capable NICs to interconnect multiple HB domains together. The conventional network architecture to interconnect HB domains is called a *rail-optimized* network (Nvidia, 2023a). GPUs within an HB domain are labeled from 1 to  $K$  as their *rank* in these networks. A *rail* is the set of GPUs with the same rank on different HB domains, interconnected with a rail switch. For instance, Figure 1 illustrates Rail 1 and Rail  $K$  in red and yellow, respectively. These rail switches are connected to spine switches subsequently to form a full-bisection any-to-any Clos network topology. This network ensures any pair of GPUs in different HB domains can communicate at the network line rate (hundreds of Gbps). For instance, traffic between GPU 1, Domain 1 and GPU 1, Domain 2 traverses through Rail Switch 1 only, while traffic between GPU 1, Domain 1 and

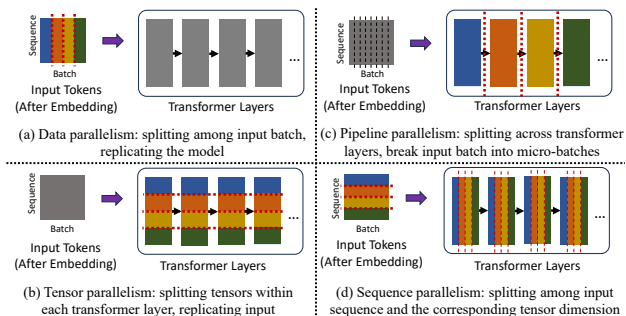


Figure 2. Different parallelization strategy for training LLMs. Each color represents a different set of devices.

GPU 2, Domain 2 goes through the respective rails and the spine switches. We refer to the connection across HB domains as the network domain in the rest of the paper.

## 2.2 Parallelization Strategies for Training LLM

The parallelization strategies of LLMs impose a profound impact on their training performance. This section dives into LLMs’ most popular parallelization strategies, from which we build our later analysis and arguments. Following prior work (Shoeybi et al., 2020; Narayanan et al., 2021; Korthikanti et al., 2022), we focus on parallelizing the chain of transformers that contributes the most to the training time.

**Data Parallelism.** Data parallelism (DP) involves distributing batches of input data across multiple GPUs, allowing each to train a replica of the DNN model simultaneously, as shown in Figure 2a. After a training iteration, the GPUs synchronize their optimizer states with an AllReduce operation, which can be overlapped with backpropagation to reduce the overhead. Scaling LLMs with DP presents a unique challenge: their model size often exceeds the memory capacity of an individual GPU, making it impossible to fit an entire model on a single processor. In this case, LLM designers employ tensor and pipeline parallelism, dividing the models across multiple GPUs to reduce the memory footprint.

**Tensor Parallelism.** Instead of dividing input data, tensor parallelism (TP) splits the model’s weight tensors (multi-dimensional data arrays) across multiple GPUs. Figure 2b illustrates TP on LLMs, in which each GPU is responsible for a portion of the tensor computations for each transformer. In particular, Shoeybi et al. (Shoeybi et al., 2020) proposed to split the model across the hidden dimension to allow parallel computation of non-linear activations. With this method of tensor spitting, a round of AllReduce is required for each attention and MLP layer for each forward and backward pass to collect the attention and gradient information, respectively. As a result, TP incurs a non-trivial amount of communication on the critical path of each tensor’s computation and requires careful planning to operate efficiently.

**Pipeline Parallelism.** For LLMs, pipeline parallelism (PP) divides the layers of the transformer and puts different layers on different devices, as illustrated in Figure 2c. In this case, each set of devices forms a pipeline stage. In addition to splitting the model, PP breaks each batch of training data into micro-batches and pipelines them across the devices. Like TP, PP reduces the per-device memory footprint by decreasing each device’s model parameters. However, PP incurs two types of overhead: the pipeline filling and draining phases (the “pipeline bubble time”) and the communication time from sending activation and gradients across pipeline stages. Most recent works on PP for LLMs use the “1F1B” schedule introduced in PipeDream (Harlap et al., 2018) to reduce the activation memory footprint. In MegatronLM, Narayanan et al. further improved this scheduling through an interleaving technique, which puts non-consecutive layers on each device and reduces the pipeline bubble time at extra communication cost (Narayanan et al., 2021).

**Sequence Parallelism.** Figure 2d shows yet another way to parallelize LLM training by splitting the training samples. Initially proposed by Li et al. (Li et al., 2022), sequence parallelism exploits the structure of LLM datasets by dividing the training samples in the sequence rather than the batch dimension to enable long-sequence training. Korthikanti et al. (Korthikanti et al., 2022) revised this approach by combining it with TP, further reducing the activation memory footprint. In this approach, the parallelism alters between the tensor (for attention and linear layers) and the sequence (for dropout and layer normalization) within a transformer. An AllGather or ReduceScatter communication re-shards the activation each time the parallelization strategy changes between TP and sequence parallelism. However, the total final communication volume for a transformer stays the same as in the TP-only case. Combining TP and sequence parallelism also reduces the PP traffic across stages since it removes the redundancy across tensor-parallel ranks, removing the requirement of the scatter-gather optimization presented in MegatronLM (Narayanan et al., 2021). In the rest of this paper, we use TP to refer to the combination of traditional TP and sequence parallelism.

## 2.3 Combining the Above: PTD-P Parallelism

Training an LLM on a large GPU cluster efficiently requires a combination of the parallelization strategies above. Narayanan et al. named such combination “PTD-P” parallelism and thoroughly analyzed the interaction of different parallelization dimensions in MegatronLM. The paper provides empirical evaluations on different parameter combinations (Narayanan et al., 2021) and derived guidelines for choosing the parallelization strategy.

PTD-P parallelism represents the state-of-the-art LLM parallelization and is widely adapted in the industry (Chowdhery

et al., 2022; Brown et al., 2020). It equally distributes the computation of the model among all GPUs while attempting to minimize the pipeline and communication overhead. However, prior work does not comprehensively analyze LLMs’ communication patterns. The following section examines the traffic pattern of training language models with PTD-P parallelism. We uncover a surprising fact: LLM training with PTD-P parallelism does not need full-bisection bandwidth connectivity in the network domain.

### 3 LLM TRAFFIC PATTERN ANALYSIS

#### 3.1 Traffic Pattern of MegatronLM

We now analyze the traffic pattern generated by LLMs with PTD-P parallelism by computing the network transfers from the model hyperparameters and the parallelization strategy. We first look at the 145.6 billion, the 310.1 billion, the 539.6 billion, and the 1 trillion parameter model described in Table 1 of MegatronLM (Narayanan et al., 2021), distributed in a cluster composed of DGX A100 servers with an HB domain of size eight. Our analysis uses the same parallelization strategy from MegatronLM to ensure optimal GPU utilization. We use the ring-based collective communication since it is bandwidth-optimal and the default algorithm in NCCL, the communication library backend of MegatronLM.

Figure 3a illustrates the volume percentage for each type of traffic for one training iteration, and Figure 3b shows the traffic type distribution across GPU pairs. There are three primary types of communication: AllGather and ReduceScatter traffic from TP, AllReduce traffic from DP, and point-to-point traffic from PP. The TP traffic happens within GPUs participating in a TP rank, which occupies an HB domain. The DP and PP traffic happen in the network domain, and their volume is significantly lesser than TP traffic, as illustrated by Figure 3a. While these types of traffic do not overlap between different pairs of GPUs, Figure 3b indicates that over 99% of GPU pairs carry *no traffic* and less than 0.04% of GPU pairs carry TP traffic. Simultaneously, Figure 3a suggests these traffic types account for over 75% of the total transmitted data. Recall that TP traffic stays within HB domains, suggesting efficient usage of HB domain bandwidth and low demand in the network domain. This pattern is consistent across all LLM models, indicating that building a cluster with any-to-any connectivity on top of HB domains for LLM models is excessive.

#### 3.2 Traffic in the Network Domain

The parallelization strategy employed in MegatronLM induced an insignificant amount of network traffic across the HB domains compared to within them. Figure 4 shows the traffic heatmap for training the GPT-1T model. In this plot, every consecutive set of eight GPUs resides within the same HB domain (highlighted in orange), and GPUs with a

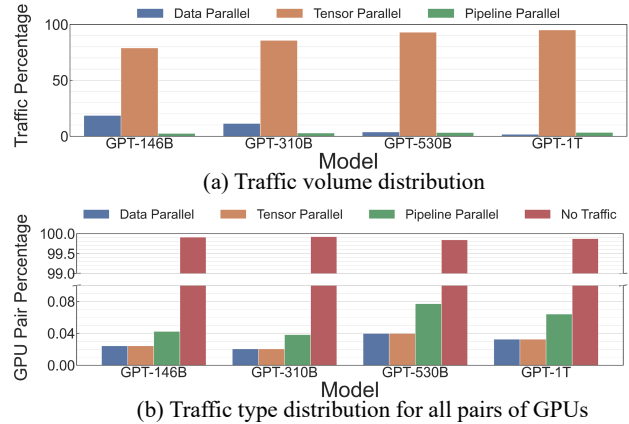


Figure 3. (a) The traffic volume from different parallelization dimensions; (b) The communication type across all GPU pairs.

distance of 8 between them belong to the same rail (highlighted in red). Figures 4a demonstrates the traffic pattern within one pipeline stage, while Figures 4b shows the traffic across the first four pipeline stages. The traffic volume is significant ( $O(100\text{ GB})$ ) across GPU pairs in an HB domain, while the communication drops to only about 6 GB across them. Furthermore, the communications across HB domains never traverse through the spine switches – these network transfers only happen within a rail.

We argue that *all* LLM distributed with an optimal PTD-P parallelization strategy always induces sparse, low-volume traffic across HB domains *within the rails*. By design, the only traffic exiting the HB domains is point-to-point traffic from pipeline parallelism or collective communication traffic (AllGather, ReduceScatter, and AllReduce) from TP and DP when DP and TP dimensions traverse beyond one HB domain. Due to the symmetry of LLM parallelization, each pipeline stage contains the same number of GPUs. As a result, the pipeline stages can always be placed such that traffic across stages always traverses on GPUs of the same rank across HB domains, hence staying within the same rail.

On the other hand, for some parallelization strategies, TP and DP can induce collective communication traffic across HB domains. For example, training a model in pure DP causes all GPUs to participate in the same DP rank and, thus, the same collective communication operation. The cluster uses hierarchical collective communication algorithms that achieve near-optimal performance in these cases.

Hierarchical collective communication algorithms are designed for a multi-tiered network topology. We introduce the method for the AllGather collective and note that ReduceScatter achieves the same performance by inverting the schedule of AllGather, and AllReduce is equivalent to a ReduceScatter followed by an AllGather. We focus on the bandwidth analysis and ignore the latency in this analysis, as the data transmission is significant during LLM training; thus, the communication runtime is bandwidth-dominated.

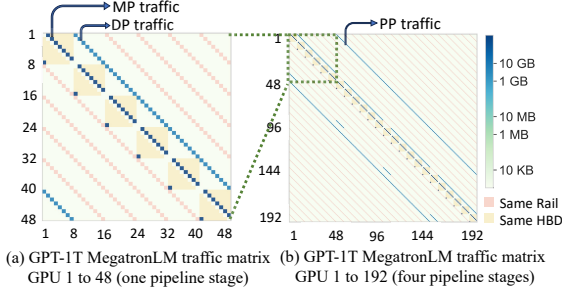


Figure 4. Traffic heatmaps for GPT-1T when applying MegatronLM’s parallelization strategy. GPUs in the same HB domains and the same rails are highlighted.

Logically, we arrange the GPUs conducting an AllGather operation into an  $x \times y$  grid, where each  $x$  GPU belongs to the same HB domain and across  $y$  total HB domains. The basic hierarchical AllGather finishes the operation in two phases: first, the algorithm collects partial data for each rail of GPUs without transferring data in the HB domain. If the total data to run AllGather is of size  $D$ , then the amount of data exchanged in the network by all GPUs is  $D(y - 1)/x$ . This operation effectively creates larger data shards for the HB domains to rerun AllGather within each HB domain. Therefore, each HB domain conducts an AllGather in the second phase, inducing a total transfer of  $D(x - 1)$ . Assume the  $x$  GPUs within an HB domain have bandwidth capacity  $C_F$  and  $y$  GPUs in the network domain have bandwidth  $C_S$ , then the total runtime is

$$\text{AGtime}(D, x, y, C_F, C_S) = \frac{(y - 1)D}{xyC_S} + \frac{(x - 1)D}{xC_F} \quad (1)$$

Like PP communication, by appropriately mapping the logical  $x \times y$  GPUs to the cluster, this algorithm only induces traffic for GPUs within the same rail. Furthermore, based on a recent result on bandwidth-optimal AllGather algorithms, we argue that as HB domain size increases, having full-bisection bandwidth in the network domain does not improve performance compared to only using connections within a rail. We defer the details of this argument to the Appendix A.

As an example with hierarchical collective communication, we now compute and analyze the traffic pattern of training the GPT-1T model, with a batch size 4096, distributed in a cluster composed of 16 Nvidia GH200 supercomputers (Nvidia, 2023b) (4096 GPUs). Each GH200 supercomputer comprises a two-tier NVSwitch architecture, facilitating 1.8 Pbps of full-bisection bandwidth (7.2 Tbps per GPU) across 256 H100 GPUs. Additionally, each GPU has a Connect-X7 HCA Infiniband network interface (Nvidia, 2023b), which provides 400 Gbps network bandwidth in/out of each GPU. In this setup, each GH200 supercomputer forms an HB domain. Figure 5 illustrates the traffic volume percentage and heatmap in this setting. The parallelization

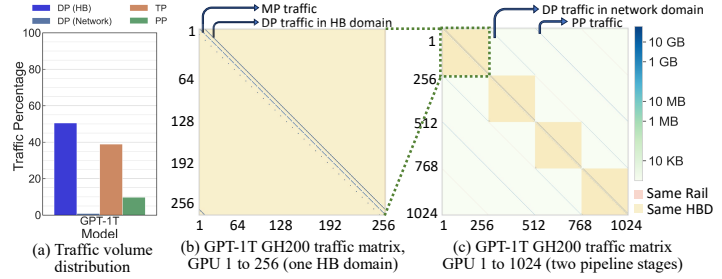


Figure 5. Traffic distribution and heatmaps for GPT-1T, distributed on 16 GH200s.

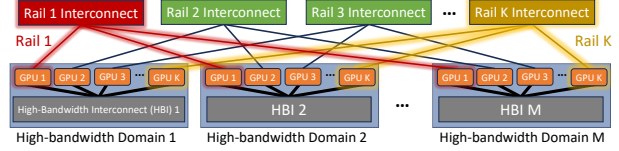


Figure 6. Our proposal: replace the any-to-any connectivity with a rail-only connection.

strategy has a total data parallel degree of 64, which spans 32 GPUs in each HB domain and two HB domains across the network. Figure 3b and 3c illustrate the traffic heatmap of the hierarchical AllReduce algorithm, which splits the AllReduce traffic among each DP group. Note that the network traffic stays within a rail (GPUs with a distance of 256 apart). The hierarchical algorithm efficiently utilized the bandwidth in the HB domain to carry 98% of the AllReduce traffic, as suggested by Figure 3a.

## 4 RAIL-ONLY NETWORK DESIGN

Based on the observations above, we propose a network architecture that diverts from the any-to-any paradigm across all GPUs. We introduce the architecture and discuss its fault-tolerant property. Figure 6 illustrates our network architecture, which we name *rail-only*. Compared to a conventional rail-optimized GPU cluster, shown in Figure 1, our network keeps the HB domains. It provides network connectivity *only within the same rail*, without changing the bandwidth. A straightforward way to realize our proposed architecture is to remove the spine switches from Figure 1 and re-purpose all the uplinks connecting rail switches to the spine as downlinks to GPUs. Hence, a dedicated but separate Clos network connects each rail. In the rest of this paper, we base our analysis on this realization of the rail-only network.

Our rail-only network architecture removes network connectivity across GPUs with different ranks in different rails. However, such communication is still possible by forwarding the data through HB domains. For instance, a message from GPU 1, Domain 1 to GPU 2, Domain 2 can first route through the first HB domain to GPU 2, Domain 1 and then be transmitted to the final destination through the network. Although our analysis shows that LLM

traffic does not require such forwarding, this connectivity might be needed for control messages, measurement, or training other DNN models in this cluster. We provide more discussions on handling other DNN models in Section 7.

#### 4.1 Fault Tolerant Properties of Rail-only Network

Fault tolerances are crucial for large GPU clusters with long-lasting LLM training jobs. This section investigates the fault tolerance properties of the rail-only network design compared to the traditional rail-optimized network.

**Link and switch failures.** Suppose a rail switch or a link fails. GPUs connected to the failed switch or link will become unavailable for either network architecture, rendering the two topologies identical regarding fault tolerance on rail switches and links. However, our design requires fewer switches, which naturally reduces the points of failure. Datacenter operators can add redundant capacity by including extra rail switches, and our design remains more cost-effective than the any-to-any network design.

**Server failure.** For a GPU cluster composed of DGX-like servers, each server forms its own HB domain. When a server fails, the network operator migrates the task to another healthy server. The rail-only connectivity remains the same for the new server. For a GH200-like cluster, a server only contains a single GPU; thus, the failure mode is the same as a single GPU failure, which we will discuss next.

#### Single GPU failures with idle GPU in the HB domain.

We discuss two distinct scenarios separately for single GPU failures. The first case is when another idle GPU presents the same HB domain as the failed one. In this case, a rail-optimized Clos network directly replaces the failed GPU with the idle one without breaking the HB domain integrity. We propose leveraging optical reconfigurable switches for the rail-only network to improve robustness. We add a small number of optical switches between the GPU and rail switches to allow reconfiguring rails dynamically. When a GPU fails, the optical switch reconfigures to bring a healthy, idle GPU to replace the failed one. This approach is conceptually similar to the failure recovery mechanism of network designs that uses optical-reconfigurable switches (Jouppi et al., 2023; Wang et al., 2023a; Poutievski et al., 2022).

#### Single GPU failure in fully occupied HB domains.

Another failure mode occurs when a GPU fails in a fully occupied HB domain and requires a substitute GPU from different HB domains. This failure mode is challenging for the rail-optimized Clos network and rail-only networks. In this case, the rail-only design prevents the straightforward solution of migrating the task to another idle GPU in the cluster, which is possible in a Clos network. However, this solution is undesirable since the new GPU no longer belongs to the same HB domain as the failed one, creating a bottleneck that

slows the HB domain into a network domain. Instead, we propose two solutions. For smaller HB domain designs (e.g.,  $K = 8$  with DGX servers), it is possible to directly migrate the entire HB domain with the failed GPU to a new one without incurring too much resource inefficiency. For larger HB domains (e.g., GH200 supercomputers with  $K = 256$ ), these HB domains are composed of a multi-tiered topology with an optical core-layer (Nvidia, 2023b). Therefore, we use the same solution as the previous case: adding optical reconfigurable switches within HB domains. When a GPU failure occurs, the optical switch reconfigures, replacing a small set of GPUs (including the failed one) with healthy ones, thus maintaining the integrity of an HB domain.

## 5 ITERATION TIME MODELING

An accurate and detailed model provides fundamental guidance for choosing the right parallelization strategy and network design. Previous research has mathematically modeled the computational time and memory requirements for various LLM training parallelization strategies (Shoeybi et al., 2020; Narayanan et al., 2021; Korthikanti et al., 2022). Nevertheless, these works omit a detailed derivation for communication time during a training iteration considering the network infrastructure. This section presents an analytical model of the training iteration time, incorporating both the parallelization strategy and the training infrastructure. This formulation is the foundation for evaluating the rail-only network design in Section 6. Table 1 outlines the parameters used in this analysis. The section assumes mixed-precision training with 16-bit model parameters, activations, and gradients.

### 5.1 Critical Path Analysis

Figure 7 displays the 1F1B pipeline schedule without interleaving. Given the uniform structure of LLMs under the PTD-P parallelism, both forward and backward execution times for each micro-batch across GPUs remain the same. This consistency allows us to identify a critical path in a training iteration, highlighted by a red arrow in Figure 7. This path further decomposes into three parts: the pipeline bubble time, the computation and communication time in the last stage (LS) of the pipeline, and finally, the parameter synchronization time after the pipeline flush. Note that the bubbling and the last pipeline stage are strictly disjointed. However, parameter synchronization traffic can start immediately for each transformer layer after the last micro-batch finishes processing, overlapping itself with the backward propagation. Another potential overlapping happens within the last stage, between the PP and TP traffic across different micro-batches. For simplicity, we provide conservative modeling of the iteration time, in which we start parameter synchronization after all computation finishes and disallow

Table 1. Parameters utilized in the calculation in this section.

Name	Description
$p, t, d$	Pipeline, Tensor and Data parallelism dimensions, respectively
$p_h, t_h, d_h$	The portion $p, t, d$ mapped into an HB domain, respectively
$p_l, t_l, d_l$	The portion $p, t, d$ mapped into the network domain, respectively
$h$	LLM Embedding dimension (hidden size)
$s$	Sequence length
$v$	Number of interleaved stages
$K$	HB domain size
$l$	Number of transformer block layers
$C_F$	HB domain bandwidth
$C_S$	GPU Network bandwidth
$S_T$	Number of parameters in a transformer block
$b$	Micro-batch size per pipeline
$m$	Number of micro-batches per iteration

cross micro-batch TP and PP traffic overlapping.

With these observations, the iteration time is

$$T_{iter} = T_{bubble} + T_{LS} + T_{sync} \quad (2)$$

This model also holds for the interleaved schedule. Interleaved schedules reduce the pipeline bubble time while requiring additional communication within the last stage of the pipeline. We factor such cost into  $T_{bubble}$  and  $T_{LS}$  in Eq. 2. The rest of this section dissects each term with explicit computation and communication cost.

## 5.2 Analytical Iteration Time Modeling

This section provides a quantitative analysis, considering each term’s computation and communication cost in Eq. 2.

**Pipeline bubble time.** For the pipeline bubble time, we break down the cost into the communication and the computation as  $T_{bubble} = T_{bubble}^{comp} + T_{bubble}^{comm}$ . Assume a micro-batch size’s total compute time (forward and backward pass) is  $t(b)$ . With interleaved scheduling of  $v$ , the computation time spent in the pipeline is

$$T_{bubble}^{comp} = \frac{(p-1)t(b)}{v} \quad (3)$$

Narayanan et al. observed that the computational efficiency of GPU varies with  $b$  (Narayanan et al., 2021); therefore, it is best to profile  $t(b)$  for each micro-batch size in practice. For simplicity, we provide an alternative measurement analytically by modeling the computational requirement (FLOPs) of an LLM and GPU’s computation speed in Appendix B.

For the communication, each micro-batch induces  $D_{\mu b}^p = 2bhs/t$  bytes of traffic across two pipeline stages when sequence parallelism is enabled together with TP. Such transfer will happen for a total of  $2(p-1)$  times throughout the pipeline filling and emptying, where  $2(p_s-1)$  times will happen in the network domain and  $2p_s(p_f-1)$  times in HB domains. Hence, the pipeline bubble communication time is

$$T_{bubble}^{comm} = \frac{2(p_s-1)D_{\mu b}^p}{C_S} + \frac{2p_s(p_f-1)D_{\mu b}^p}{C_F} \quad (4)$$

Unlike the computation time, the communication time for bubbling is unaffected by the interleaved scheduling.

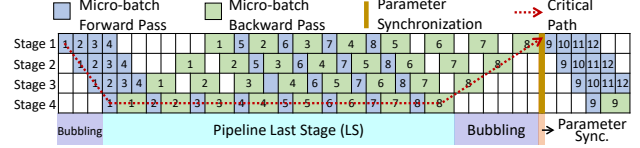


Figure 7. 1F1B pipeline schedule and its critical path.

**Last stage time.** Similar to the bubble time, we analyze the computation and computation costs separately in the last stage of the pipeline. The last stage has  $m$  micro-batches going through it, and therefore the computational cost is

$$T_{LS}^{comp} = mt(b) \quad (5)$$

For communication, TP and PP both generate network traffic across GPUs. We first focus on the TP traffic: for each micro-batch, four AllGather and four ReduceScatter happen in total for each layer of the transformer layer when sequence parallelism is applied. Since ReduceScatter is the inverse of AllGather and generates the same amount of traffic, this analysis will focus on AllGather only. Recall  $\text{AGtime}(D, x, y, C_F, C_S)$  (Eq. 1) is the time of running AllGather on data of size  $D$  bytes on an  $x \times y$  grid of GPUs with HB domain and network bandwidth  $C_F, C_S$  respectively. The amount of data to run AllGather for each micro-batch is  $D_{\mu b}^t = 2bhs$  per transformer block, and since each pipeline stage holds  $l/p$  transformer blocks, the total runtime for all  $m$  micro-batches is  $8lm\text{AGtime}(D_{\mu b}^t, t_h, t_l, C_F, C_S)/p$ .

Next, we look at the pipeline traffic in the last stage. The pipeline traffic can overlap with the computation, even with interleaved scheduling; however, with conservative modeling, we assume that GPUs do not perform computation when sending and receiving pipeline parallel traffic. Each interleaved part of each micro-batch at least sends or receives  $D_{\mu b}^p$  bytes of traffic both on the forward and backward pass and every micro-batch needs to traverse the network domain whenever  $p_s > 1$ . Therefore, we model the pipeline communication overhead in the last stage as  $2mvD_{\mu b}^p/C_*$  where  $C_* = C_S$  if  $p_s > 1$ , else  $C_* = C_F$ . Adding the tensor and pipeline communication time together,

$$T_{LS}^{comm} = \frac{8lm\text{AGtime}(D_{\mu b}^t, t_h, t_l, C_F, C_S)}{p} + \frac{2mvD_{\mu b}^p}{C_*} \quad (6)$$

**Parameter Synchronization.** Finally, we have the parameter synchronization time, consisting of an AllReduce operation of the model parameters in the first stage of the pipeline. We only model the communication time of the AllReduce operation since the computation of AllReduce incurs minimal overhead. We follow the same hierarchical collective algorithm described in Section 4. For a  $d = d_h \times d_l$  way DP, the amount of data to AllReduce is  $D^d = 2lS_T/pt$ . An AllReduce induces twice the runtime as an AllGather for

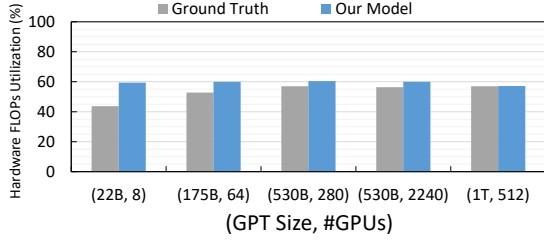


Figure 8. HFU comparison between the ground truth (Korthikanti et al., 2022) and our formulation.

the same amount of data; therefore,

$$T_{sync} = 2AGtime(D^d, d_h, d_l, C_F, C_S) \quad (7)$$

Together, Eq. 3, 4, 5, 6 and 7 provide a closed-form expression for Eq. 2 as the training iteration time for an LLM. While this section only presents the transmission delay, in our evaluation, we also consider the propagation delay (network latency) for the communication times to get the best iteration time accuracy.

### 5.3 Constraints in Choosing Parameters

In addition to the cost model, we derive the set of constraints of the hyperparameters that describe a complete parallelization strategy. We derive a program that exhaustively generates all the possible parallelization configurations in Appendix C. The iteration time model from Eq. 2 then serves as the cost of an optimization problem to derive the optimal parallelization strategy. In the next section, we evaluate the accuracy of this modeling and use it as the basis for analyzing our rail-only network design for training LLMs.

## 6 EVALUATION

### 6.1 Accuracy of the Iteration Time Modeling

We evaluate the accuracy of our iteration time model from Section 5 by comparing the computed hardware FLOPs utilization (HFU) against testbed results from previous work. The HFU refers to the hardware’s floating point operation performed in an iteration over the peak floating point operations. The paper from Korthikanti et al. (Korthikanti et al., 2022) provides the full set of hyperparameters in their evaluation setup (replicated in Appendix E) and allows us to compare the estimated HFU to the ground truth directly. The infrastructure consists of DGX A100 servers. We follow the formula presented by Korthikanti et al. (Korthikanti et al., 2022) to compute the total FLOP of training with selective activation recomputation.

The discrepancy between the mathematical model and the ground truth comes from the idealistic modeling of GPU computation and communication, the assumptions on how computation and communication overlap, and ignoring the overhead of memory operations. Figure 8 illustrates the

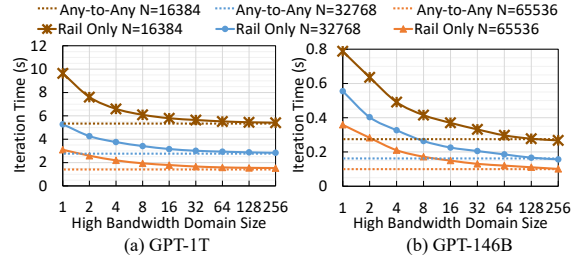


Figure 9. Iteration time as HB domain size changes.

comparison result for different GPT models and cluster scales. As the LLM size increases, our formulation’s accuracy increases, and for GPT-1T, our computed HFU only differs from the ground truth by 0.15%. This reduction is because a larger LLM utilizes the computation resource more efficiently, resulting in a more accurate estimation of the computation time for each micro-batch. The worst-case estimation comes from the smallest GPT-22B model, with a difference of 15.7% in computed and ground truth MFU. We note that discrete event simulations are not scalable at the cluster size of our evaluation. On the other hand, a coarse-grain flow simulation based on the mathematical modeling of the system will produce a similar result as Eq. 2 does. Therefore, the rest of this section utilizes the mathematical model to evaluate the training iteration time.

### 6.2 What is the Ideal Size of an HB Domain?

Increasing HB domain size reduces the network overhead of a training iteration. The question that naturally follows the rail-only network design process is, *what should be the ideal size of the HB domain?* In Figure 9, we vary the HB domain size ( $K$ ) and plot the training iteration time for GPT-1T and GPT-146B from MegatronLM for clusters of 16384, 32768, and 65536 H100 GPUs. The global batch size in this evaluation is 4096 and 1024, respectively. We use the optimal parallelization strategy found with our formulation for each cluster size, using the bandwidth and computational ability parameters of GH200. We also compute the ideal-case performance of the “Any-to-Any NVLink” training iteration time. This design point represents the idealized scenario where a full-bisection NVLink fabric connects every GPU or the case where  $K = N$ , where  $N$  is the total GPU count.

As depicted in Figure 9, the iteration time goes down as the HB domain size increases, indicating that larger HB domains reduce the network overhead of training. However, the *performance gain* decreases as the HB domain size increases. For the larger GPT-1T model, increasing HB domain size from one (i.e., all GPUs connected with only the network domain) to eight sees an average gain of 36.5%. In contrast, an increment from 8 to 256 realizes a gain of 16.3%. This reduction in communication time gain can be attributed to Amdahl’s law, as the computation time of the DNN remains constant across all instances.



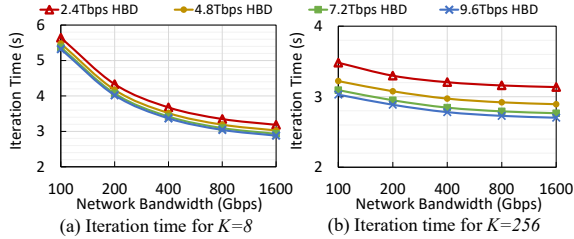


Figure 10. Iteration time of GPT-1T as HB domain bandwidth and network bandwidth varies for different HB domain sizes.

For the smaller GPT-146B model, the performance gain of increasing HB domain size is higher than that of GPT-1T. Providing an HB domain of size eight realizes a 50.6% performance gain compared to the HB domain of size one, while increasing the HB domain size from 8 to 256 further achieves a 39.1% gain. We reveal that smaller LLMs incur more communication overhead when distributed to the same cluster than larger models. This effect arises from how computation and communication costs scale as LLM grows. As the analysis in Section 5 suggests, the communication requirement increases linearly with the model’s hidden size and sequence length. On the other hand, the model FLOPs increase quadratically with these two parameters, as indicated by previous work (Narayanan et al., 2021).

However, in both GPT models, the performance achieved with an HB domain size of 256 is nearly optimal. Compared to the ideal case, GPT-146B with an HB domain of 256 is 8.9% slower, while GPT-1T is 1.3% slower in this case. We argue that the current GH200 supercomputer, with an HB domain of size 256, is well-suited to the demands of LLM training today, especially as LLMs get larger. At the same time, prospective technological advancements augmenting this size will further benefit the training performance, especially for smaller models, reducing the training iteration time closer to the ideal case without requiring any-to-any connectivity in the network across HB domains.

### 6.3 Impact of HB Domain and Network Bandwidth

The bandwidth of HB and network domains fundamentally determines the communication time. We analyze the impact of these bandwidths on LLM’s iteration time. Figure 10a and 10b show the iteration time variation for different HB domain bandwidths (different lines) and network bandwidths in the rails (on the  $x$ -axis), for  $K = 8$  and 256, respectively. As expected, the iteration time drops when either bandwidth increases. However, the  $K = 8$  case is less sensitive to the HB domain bandwidth. Increasing the per-GPU bandwidth by a factor of four (from 2.4 Tbps to 9.6 Tbps) only improves the iteration time by 8.0% on average for  $K = 8$ , compared to the improvement of 13.3% for  $K = 256$ . On the other hand, larger HB domain sizes are less sensitive to network bandwidth improvement. Increasing the bandwidth from 100 Gbps to 400 Gbps, also

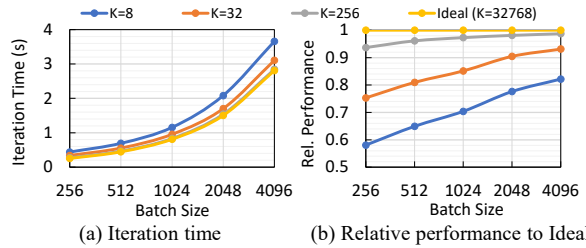


Figure 11. Iteration time and relative performance to the ideal case, as batch size changes, for GPT-1T.

a factor of four, results in 35.9% improvement for  $K = 8$  but only 8.0% for  $K = 256$ . While increasing either bandwidth consists of separate efforts on the hardware, as HB domain size goes up, improving the HB domain bandwidth is more beneficial than the network bandwidth for LLMs as future HB domain size increases.

### 6.4 Impact of Batch Size on Network Design

While the batch size is typically an ML-centric metric for optimization, our analysis indicates that the impact of batch size on the comprehensive training performance goes beyond the total number of iterations required for convergence. To further understand the impact of batch size on training time, we analyze the performance of a GPT-1T model on a 32768 GPU cluster while changing the HB domain size from  $K = 8$  to 32768. We vary the global batch size from 256 to 4096 in this study. Figure 11a plots the change in iteration time as the batch size varies. The iteration time exhibits a similar trajectory for all HB domain sizes; however, the *relative performance* (the ratio to the iteration time for an HB domain size to that of the ideal case) improves as the batch size increases. Figure 11b represents this trend. When  $K = 256$ , the relative performance increases from 93% to 99% as the batch size increases from 256 to 4096 sequences. This result also supports that  $K = 256$  provides a near-optimal performance. This effect is prominent when the HB domain size is small. For  $K = 8$ , increasing the batch size from 256 to 4096 improves the relative performance from 58% to 82%, suggesting a larger batch size is preferable for a cluster with a smaller HB domain. Prior studies have shown that LLM training benefits from a larger batch size (Kaplan et al., 2020; Brown et al., 2020), especially for bigger models, making it a perfect fit for our rail-only design.

### 6.5 Network Cost Analysis

Our rail-only network architecture judiciously reduces the network resources for LLM training by eliminating unused network connections. This section compares the network cost of our proposed approach with the state-of-the-art rail-optimized GPU clusters. We calculate the number of switches (#SW) and transceivers (#TR) required for each network design and derive the network equipment cost based

Table 2. Number of switches for different clusters.

#GPUs (N)	Switch Radix	SOTA #SW	Rail-only #SW	SOTA #TR	Rail-only #TR	Cost Reduction
32768	64	2560	1536	196608	131072	37%
	128	1280	256	196608	65536	75%
	256	384	128	131072	65536	60%
65536	64	5120	3072	393216	262144	37%
	128	2560	1536	393216	262144	37%
	256	1280	256	393216	131072	75%

on numbers reported in prior work (Wang et al., 2023a)<sup>1</sup>. We enumerate the number of switches and transceivers required to build the state-of-the-art network architecture and our proposed architecture in Table 2, accounting for variable cluster sizes and network switch radix. Note that for the state-of-the-art architecture, each rail of GPUs is not physically separated in some cases to use the least amount of network resources. Thus, the datacenter operator must manually configure the switch to achieve the desired isolation across rails to achieve the rail-optimized design.

The last column of Table 2 illustrates our design’s cost savings over the state-of-the-art for the total cost of switches and transceivers. Our rail-only design notably reduces the network cost by 37% to 75% compared to the state-of-the-art design while achieving equivalent performance. This reduction stems from eliminating core layer switches and decreasing the number of switch tiers within each rail. Surprisingly, switches with a radix of 64 provide the worst-case cost reduction in both cluster sizes. In this case, the state-of-the-art design requires a three-tier Clos network, while the rail-only design requires two tiers for each rail. Still, our design only requires three-quarters of the total number of switches while achieving the same performance as the state-of-the-art design.

## 7 RELATED WORK

**LLM trend.** The current growth rate of LLM computational and speed requirement outpaces the advancements in AI accelerators and network speed as Moore’s law slows down, necessitating hyper-scale clusters and more efficient interconnects (Ballani et al., 2020; OpenAI, 2023a). The MegatronLM line of work pioneers LLM parallelization (Shoeybi et al., 2020; Narayanan et al., 2021; Korthikanti et al., 2022). Our position to remove any-to-any network connectivity complements MegatronLM. We also acknowledge ongoing efforts to reduce language models’ size and resource requirements without compromising performance (Databricks, 2023). These works complement ours as our design reduces network resources and maintains performance even for smaller language models and clusters. Similarly, research directions that aim to directly reduce the amount of communication through quantization and compression, like DeepSpeed Zero++, also complement our

<sup>1</sup>\$374 per transceiver, \$748 per switch port for 400 Gbps.

approach (Microsoft, 2023). Another trend deviates from the dense LLM model through the Mixture-of-Expert (MoE) method (Rajbhandari et al., 2022; Artetxe et al., 2022; Fedus et al., 2022), which potentially induces All-to-All traffic in the network domain. In this case, LLM designers can use host-based forwarding or an algorithm like the hierarchical All-to-All presented in DeepSpeed MoE (Rajbhandari et al., 2022), achieving a worst-case communication performance penalty of factor  $C_F/C_S$  (Appendix D) compared to a full-bisection rail-optimized network.

**LLM Inference.** This paper explores the training workload of LLMs, yet inference represents another significant part of the LLM product cycle. Inference demands fewer resources as it involves moving less data through the LLM and only computes the forward pass and multiple passes to generate response tokens (Li et al., 2023). Pope et al. developed specific parallelism for inference on TPU-v4 architecture (Pope et al., 2022). For our design, each HB domain becomes an inference-serving domain with low latency, and the rail-only connections help load-balance multiple inference domains. We leave a detailed investigation of LLM inference to future work.

**Multi-job training.** It is common for a GPU cluster to train multiple smaller jobs simultaneously. Existing works focus on Clos-based GPU clusters and provide techniques for better fairness and shorter job-completion time (Xiao et al., 2018; Gu et al., 2019; Zhao et al., 2022b; Rajasekaran et al., 2023). While this paper focuses on training a single LLM on a large cluster, the rail-only network design is also suitable for a multi-job setting. The entire cluster can be arbitrarily partitioned by tiling into smaller rectangular partitions, similar to the case of TPU-v4 (Jouppi et al., 2023). Each partition then independently executes a smaller training job.

**ML infrastructures and other ML workloads.** Prior works illustrated the benefits of co-designing hardware and software for ML models. For instance, Google’s TPU cluster is optimized for training large models with 3D parallelism on TPUs (Jouppi et al., 2023), while Meta’s Neo focuses on training recommendation models with large embedding tables (Mudigere et al., 2023). To the best of our knowledge, our work is the first to focus on designing a cost-efficient network to train LLMs efficiently. Although our proposed rail-only architecture focuses on network design specifically for LLMs, our design is efficient for many other DNN workloads when combined with other efforts. Recent works attempt to make the parallelization strategy and collective communication algorithms bandwidth-aware for any DNN model (Zheng et al., 2022; Unger et al., 2022; Zhao & Krishnamurthy, 2023), which already produce traffic patterns resembling that of LLMs. The cluster uses forwarding described in Section 4 for parallelization strategies requiring communication across the rails.

## 8 CONCLUSION

This paper challenges the conventional any-to-any network architecture for GPU clusters for training large language models. We propose a new *rail-only architecture* that aligns with LLMs’ distinct characteristics and demands, leading to 37% to 75% cost reductions while maintaining identical performance to the current state-of-the-art Clos networks.

## REFERENCES

- Artetxe, M., Bhosale, S., Goyal, N., Mihaylov, T., Ott, M., Shleifer, S., Lin, X. V., Du, J., Iyer, S., Pasunuru, R., Anantharaman, G., Li, X., Chen, S., Akin, H., Baines, M., Martin, L., Zhou, X., Koura, P. S., O’Horo, B., Wang, J., Zettlemoyer, L., Diab, M., Kozareva, Z., and Stoyanov, V. Efficient large scale language modeling with mixtures of experts, 2022.
- Bai, W., Abdeen, S. S., Agrawal, A., Attre, K. K., Bahl, P., Bhagat, A., Bhaskara, G., Brokhman, T., Cao, L., Cheema, A., Chow, R., Cohen, J., Elhaddad, M., Ette, V., Figlin, I., Firestone, D., George, M., German, I., Ghai, L., Green, E., Greenberg, A., Gupta, M., Haagens, R., Hendel, M., Howlader, R., John, N., Johnstone, J., Jolly, T., Kramer, G., Kruse, D., Kumar, A., Lan, E., Lee, I., Levy, A., Lipshteyn, M., Liu, X., Liu, C., Lu, G., Lu, Y., Lu, X., Makhervaks, V., Malashanka, U., Maltz, D. A., Marinos, I., Mehta, R., Murthi, S., Namdhari, A., Ogus, A., Padhye, J., Pandya, M., Phillips, D., Power, A., Puri, S., Raindel, S., Rhee, J., Russo, A., Sah, M., Sheriff, A., Sparacino, C., Srivastava, A., Sun, W., Swanson, N., Tian, F., Tomczyk, L., Vadlamuri, V., Wolman, A., Xie, Y., Yom, J., Yuan, L., Zhang, Y., and Zill, B. Empowering azure storage with RDMA. In *20th USENIX Symposium on Networked Systems Design and Implementation (NSDI 23)*, pp. 49–67, Boston, MA, April 2023. USENIX Association. ISBN 978-1-939133-33-5. URL <https://www.usenix.org/conference/nsdi23/presentation/bai>.
- Bai, Y., Li, C., Zhou, Q., Yi, J., Gong, P., Yan, F., Chen, R., and Xu, Y. Gradient compression supercharged high-performance data parallel dnn training. In *Proceedings of the ACM SIGOPS 28th Symposium on Operating Systems Principles, SOSP ’21*, pp. 359–375, New York, NY, USA, 2021. Association for Computing Machinery. ISBN 9781450387095. doi: 10.1145/3477132.3483553. URL <https://doi.org/10.1145/3477132.3483553>.
- Ballani, H., Costa, P., Behrendt, R., Cletheroe, D., Haller, I., Jozwik, K., Karinou, F., Lange, S., Shi, K., Thomson, B., and Williams, H. Sirius: A flat datacenter network with nanosecond optical switching. In *Proceedings of the Annual Conference of the ACM Special Interest Group on Data Communication on the Applications, Technologies, Architectures, and Protocols for Computer Communication, SIGCOMM ’20*, pp. 782–797, New York, NY, USA, 2020. Association for Computing Machinery. ISBN 9781450379557. doi: 10.1145/3387514.3406221. URL <https://doi.org/10.1145/3387514.3406221>.
- Brown, T. B., Mann, B., Ryder, N., Subbiah, M., Kaplan, J., Dhariwal, P., Neelakantan, A., Shyam, P., Sastry, G., Askell, A., Agarwal, S., Herbert-Voss, A., Krueger, G., Henighan, T., Child, R., Ramesh, A., Ziegler, D. M., Wu, J., Winter, C., Hesse, C., Chen, M., Sigler, E., Litwin, M., Gray, S., Chess, B., Clark, J., Berner, C., McCandlish, S., Radford, A., Sutskever, I., and Amodei, D. Language models are few-shot learners, 2020.
- Chowdhery, A., Narang, S., Devlin, J., Bosma, M., Mishra, G., Roberts, A., Barham, P., Chung, H. W., Sutton, C., Gehrmann, S., Schuh, P., Shi, K., Tsvyashchenko, S., Maynez, J., Rao, A., Barnes, P., Tay, Y., Shazeer, N., Prabhakaran, V., Reif, E., Du, N., Hutchinson, B., Pope, R., Bradbury, J., Austin, J., Isard, M., Gur-Ari, G., Yin, P., Duke, T., Levskaya, A., Ghemawat, S., Dev, S., Michalewski, H., Garcia, X., Misra, V., Robinson, K., Fedus, L., Zhou, D., Ippolito, D., Luan, D., Lim, H., Zoph, B., Spiridonov, A., Sepassi, R., Dohan, D., Agrawal, S., Omernick, M., Dai, A. M., Pillai, T. S., Pellat, M., Lewkowycz, A., Moreira, E., Child, R., Polozov, O., Lee, K., Zhou, Z., Wang, X., Saeta, B., Diaz, M., Firat, O., Catasta, M., Wei, J., Meier-Hellstern, K., Eck, D., Dean, J., Petrov, S., and Fiedel, N. Palm: Scaling language modeling with pathways, 2022.
- Dao, T. Flashattention-2: Faster attention with better parallelism and work partitioning, 2023.
- Databricks. Hello dolly: Democratizing the magic of chatgpt with open models, 2023. URL <https://www.databricks.com/blog/2023/03/24/hello-dolly-democratizing-magic-chatgpt-open-models.html>.
- Fedus, W., Zoph, B., and Shazeer, N. Switch transformers: Scaling to trillion parameter models with simple and efficient sparsity, 2022.
- Goyal, P., Shah, P., Zhao, K., Nikolaidis, G., Alizadeh, M., and Anderson, T. E. Backpressure flow control. In *19th USENIX Symposium on Networked Systems Design and Implementation (NSDI 22)*, pp. 779–805, Renton, WA, April 2022. USENIX Association. ISBN 978-1-939133-27-4. URL <https://www.usenix.org/conference/nsdi22/presentation/goyal>.
- Gu, J., Chowdhury, M., Shin, K. G., Zhu, Y., Jeon, M., Qian, J., Liu, H., and Guo, C. Tiresias: A

- GPU cluster manager for distributed deep learning. In *16th USENIX Symposium on Networked Systems Design and Implementation (NSDI 19)*, pp. 485–500, Boston, MA, February 2019. USENIX Association. ISBN 978-1-931971-49-2. URL <https://www.usenix.org/conference/nsdi19/presentation/gu>.
- Guo, C., Wu, H., Deng, Z., Soni, G., Ye, J., Padhye, J., and Lipshteyn, M. Rdma over commodity ethernet at scale. In *Proceedings of the 2016 ACM SIGCOMM Conference, SIGCOMM '16*, pp. 202–215, New York, NY, USA, 2016. Association for Computing Machinery. ISBN 9781450341936. doi: 10.1145/2934872.2934908. URL <https://doi.org/10.1145/2934872.2934908>.
- Harlap, A., Narayanan, D., Phanishayee, A., Seshadri, V., Devanur, N., Ganger, G., and Gibbons, P. Pipedream: Fast and efficient pipeline parallel dnn training, 2018.
- Hu, S., Zhu, Y., Cheng, P., Guo, C., Tan, K., Padhye, J., and Chen, K. Deadlocks in datacenter networks: Why do they form, and how to avoid them. In *Proceedings of the 15th ACM Workshop on Hot Topics in Networks, HotNets '16*, pp. 92–98, New York, NY, USA, 2016. Association for Computing Machinery. ISBN 9781450346610. doi: 10.1145/3005745.3005760. URL <https://doi.org/10.1145/3005745.3005760>.
- Jia, Z., Zaharia, M., and Aiken, A. Beyond data and model parallelism for deep neural networks. *SysML*, 2019. URL <https://mlsys.org/Conferences/2019/doc/2019/16.pdf>.
- Jouppi, N. P., Kurian, G., Li, S., Ma, P., Nagarajan, R., Nai, L., Patil, N., Subramanian, S., Swing, A., Towles, B., Young, C., Zhou, X., Zhou, Z., and Patterson, D. Tpu v4: An optically reconfigurable supercomputer for machine learning with hardware support for embeddings, 2023.
- Kaplan, J., McCandlish, S., Henighan, T., Brown, T. B., Chess, B., Child, R., Gray, S., Radford, A., Wu, J., and Amodei, D. Scaling laws for neural language models, 2020.
- Khani, M., Ghobadi, M., Alizadeh, M., Zhu, Z., Glick, M., Bergman, K., Vahdat, A., Klenk, B., and Ebrahimi, E. Sip-ml: High-bandwidth optical network interconnects for machine learning training. In *Proceedings of the 2021 ACM SIGCOMM 2021 Conference, SIGCOMM '21*, pp. 657–675, New York, NY, USA, 2021. Association for Computing Machinery. ISBN 9781450383837. doi: 10.1145/3452296.3472900. URL <https://doi.org/10.1145/3452296.3472900>.
- Korthikanti, V., Casper, J., Lym, S., McAfee, L., Andersch, M., Shoeybi, M., and Catanzaro, B. Reducing activation recomputation in large transformer models, 2022.
- Labs, L. Openai’s gpt-3 language model: A technical overview, 2020. URL <https://lambdalabs.com/blog/demystifying-gpt-3>.
- Li, S., Xue, F., Baranwal, C., Li, Y., and You, Y. Sequence parallelism: Long sequence training from system perspective, 2022.
- Li, Z., Zheng, L., Zhong, Y., Liu, V., Sheng, Y., Jin, X., Huang, Y., Chen, Z., Zhang, H., Gonzalez, J. E., and Stoica, I. AlpaServe: Statistical multiplexing with model parallelism for deep learning serving. In *17th USENIX Symposium on Operating Systems Design and Implementation (OSDI 23)*, Boston, MA, July 2023. USENIX Association. URL <https://www.usenix.org/conference/osdi23/presentation/li-zhouhan>.
- Meta. Meta platforms is determined to make ethernet work for ai, 2023. URL <https://www.nextplatform.com/2023/09/26/meta-platforms-is-determined-to-make-ethernet-work-for-ai/>.
- Microsoft. Deepspeed zero++: A leap in speed for llm and chat model training with 4x less communication, 2023. URL <https://www.microsoft.com/en-us/research/blog/deepspeed-zero-a-leap-in-speed-for-llm-and-chat-model-training-with-4x-less-communication/>.
- Mittal, R., Shpiner, A., Panda, A., Zahavi, E., Krishnamurthy, A., Ratnasamy, S., and Shenker, S. Revisiting network support for rdma. In *Proceedings of the 2018 Conference of the ACM Special Interest Group on Data Communication, SIGCOMM '18*, pp. 313–326, New York, NY, USA, 2018. Association for Computing Machinery. ISBN 9781450355674. doi: 10.1145/3230543.3230557. URL <https://doi.org/10.1145/3230543.3230557>.
- Mudigere, D., Hao, Y., Huang, J., Jia, Z., Tulloch, A., Sridharan, S., Liu, X., Ozdal, M., Nie, J., Park, J., Luo, L., Yang, J. A., Gao, L., Ivchenko, D., Basant, A., Hu, Y., Yang, J., Ardestani, E. K., Wang, X., Komuravelli, R., Chu, C.-H., Yilmaz, S., Li, H., Qian, J., Feng, Z., Ma, Y., Yang, J., Wen, E., Li, H., Yang, L., Sun, C., Zhao, W., Melts, D., Dhulipala, K., Kishore, K., Graf, T., Eisenman, A., Matam, K. K., Gangidi, A., Chen, G. J., Krishnan, M., Nayak, A., Nair, K., Muthiah, B., khorashadi, M., Bhattacharya, P., Lapukhov, P., Naumov, M., Mathews, A., Qiao, L., Smelyanskiy, M., Jia, B., and Rao, V. Software-hardware co-design for fast and scalable training of deep learning recommendation models. In *Proceedings of the 49th Annual International Symposium on Computer Architecture, ISCA '22*, pp. 993–1011, New York, NY, USA, 2022. Association for

- Computing Machinery. ISBN 9781450386104. doi: 10.1145/3470496.3533727. URL <https://doi.org/10.1145/3470496.3533727>.
- Mudigere, D., Hao, Y., Huang, J., Jia, Z., Tulloch, A., Sridharan, S., Liu, X., Ozdal, M., Nie, J., Park, J., Luo, L., Yang, J. A., Gao, L., Ivchenko, D., Basant, A., Hu, Y., Yang, J., Ardestani, E. K., Wang, X., Komuravelli, R., Chu, C.-H., Yilmaz, S., Li, H., Qian, J., Feng, Z., Ma, Y., Yang, J., Wen, E., Li, H., Yang, L., Sun, C., Zhao, W., Melts, D., Dhulipala, K., Kishore, K., Graf, T., Eisenman, A., Matam, K. K., Gangidi, A., Chen, G. J., Krishnan, M., Nayak, A., Nair, K., Muthiah, B., khorashadi, M., Bhattacharya, P., Lapukhov, P., Naumov, M., Mathews, A., Qiao, L., Smelyanskiy, M., Jia, B., and Rao, V. Software-hardware co-design for fast and scalable training of deep learning recommendation models, 2023.
- Narayanan, D., Shoeybi, M., Casper, J., LeGresley, P., Patwary, M., Korthikanti, V. A., Vainbrand, D., Kashinkunti, P., Bernauer, J., Catanzaro, B., Phanishayee, A., and Zaharia, M. Efficient large-scale language model training on gpu clusters using megatron-lm, 2021.
- Nvidia. Nvidia dgx superpod: Next generation scalable infrastructure for ai leadership, reference architecture, 2023a. URL <https://docs.nvidia.com/dgx-superpod-reference-architecture-with-dgx-h100-systems.pdf>.
- Nvidia. Nvidia dgx gh200, 2023b. URL <https://www.nvidia.com/en-us/data-center/dgx-gh200/>.
- Nvidia. Nvidia gpudirect: Enhancing data movement and access for gpus, 2023c. URL <https://developer.nvidia.com/gpudirect>.
- Nvidia. Nvlink and nvswitch: The building blocks of advanced multi-gpu communication—within and between servers., 2023d. URL <https://www.nvidia.com/en-us/data-center/nvlink/>.
- OpenAI. Openai: Ai and compute, 2023a. URL <https://openai.com/research/ai-and-compute>.
- OpenAI. Gpt-4 technical report, 2023b.
- Pope, R., Douglas, S., Chowdhery, A., Devlin, J., Bradbury, J., Levskaya, A., Heek, J., Xiao, K., Agrawal, S., and Dean, J. Efficiently scaling transformer inference, 2022.
- Poutievski, L., Mashayekhi, O., Ong, J., Singh, A., Tariq, M., Wang, R., Zhang, J., Beauregard, V., Conner, P., Gribble, S., Kapoor, R., Kratzer, S., Li, N., Liu, H., Nagaraj, K., Ornstein, J., Sawhney, S., Urata, R., Visciano, L., Yasumura, K., Zhang, S., Zhou, J., and Vahdat, A. Jupiter evolving: Transforming google’s datacenter network via optical circuit switches and software-defined networking. In *Proceedings of the ACM SIGCOMM 2022 Conference, SIGCOMM ’22*, pp. 66–85, New York, NY, USA, 2022. Association for Computing Machinery. ISBN 9781450394208. doi: 10.1145/3544216.3544265. URL <https://doi.org/10.1145/3544216.3544265>.
- Rajasekaran, S., Ghobadi, M., and Akella, A. Cassini: Network-aware job scheduling in machine learning clusters, 2023.
- Rajbhandari, S., Li, C., Yao, Z., Zhang, M., Aminabadi, R. Y., Awan, A. A., Rasley, J., and He, Y. Deepspeed-moe: Advancing mixture-of-experts inference and training to power next-generation ai scale, 2022.
- Schneider, T., Bibartiu, O., and Hoeffler, T. Ensuring deadlock-freedom in low-diameter infiniband networks. In *2016 IEEE 24th Annual Symposium on High-Performance Interconnects (HOTI)*, pp. 1–8, 2016. doi: 10.1109/HOTI.2016.015.
- Shainer, G., Lui, P., and Liu, T. The development of mellanox/nvidia gpudirect over infiniband: A new model for gpu to gpu communications. In *Proceedings of the 2011 TeraGrid Conference: Extreme Digital Discovery, TG ’11*, New York, NY, USA, 2011. Association for Computing Machinery. ISBN 9781450308885. doi: 10.1145/2016741.2016769. URL <https://doi.org/10.1145/2016741.2016769>.
- Shoeybi, M., Patwary, M., Puri, R., LeGresley, P., Casper, J., and Catanzaro, B. Megatron-lm: Training multi-billion parameter language models using model parallelism, 2020.
- The-Decoder. Gpt-4 has a trillion parameters - report, 2023. URL <https://the-decoder.com/gpt-4-has-a-trillion-parameters/>.
- Touvron, H., Lavril, T., Izacard, G., Martinet, X., Lachaux, M.-A., Lacroix, T., Rozière, B., Goyal, N., Hambro, E., Azhar, F., Rodriguez, A., Joulin, A., Grave, E., and Lample, G. Llama: Open and efficient foundation language models, 2023.
- Unger, C., Jia, Z., Wu, W., Lin, S., Baines, M., Narvaez, C. E. Q., Ramakrishnaiah, V., Prajapati, N., McCormick, P., Mohd-Yusof, J., Luo, X., Mudigere, D., Park, J., Smelyanskiy, M., and Aiken, A. Unity: Accelerating DNN training through joint optimization of algebraic transformations and parallelization. In *16th USENIX Symposium on Operating Systems Design and Implementation (OSDI 22)*, pp. 267–284, Carlsbad, CA, July 2022. USENIX Association. ISBN 978-1-939133-28-1. URL <https://www.usenix.org/conference/osdi22/presentation/unger>.

- Wang, M., Huang, C.-c., and Li, J. Supporting very large models using automatic dataflow graph partitioning. In *Proceedings of the Fourteenth EuroSys Conference 2019*, EuroSys '19, New York, NY, USA, 2019. Association for Computing Machinery. ISBN 9781450362818. doi: 10.1145/3302424.3303953. URL <https://doi.org/10.1145/3302424.3303953>.
- Wang, W., Khazraee, M., Zhong, Z., Ghobadi, M., Jia, Z., Mudigere, D., Zhang, Y., and Kewitsch, A. TopoOpt: Co-optimizing network topology and parallelization strategy for distributed training jobs. In *20th USENIX Symposium on Networked Systems Design and Implementation (NSDI 23)*, pp. 739–767, Boston, MA, April 2023a. USENIX Association. ISBN 978-1-939133-33-5. URL <https://www.usenix.org/conference/nsdi23/presentation/wang-weiyang>.
- Wang, Z., Luo, L., Ning, Q., Zeng, C., Li, W., Wan, X., Xie, P., Feng, T., Cheng, K., Geng, X., Wang, T., Ling, W., Huo, K., An, P., Ji, K., Zhang, S., Xu, B., Feng, R., Ding, T., Chen, K., and Guo, C. SRNIC: A scalable architecture for RDMA NICs. In *20th USENIX Symposium on Networked Systems Design and Implementation (NSDI 23)*, pp. 1–14, Boston, MA, April 2023b. USENIX Association. ISBN 978-1-939133-33-5. URL <https://www.usenix.org/conference/nsdi23/presentation/wang-zilong>.
- Xiao, W., Bhardwaj, R., Ramjee, R., Sivathanu, M., Kwatra, N., Han, Z., Patel, P., Peng, X., Zhao, H., Zhang, Q., Yang, F., and Zhou, L. Gandiva: Introspective cluster scheduling for deep learning. In *13th USENIX Symposium on Operating Systems Design and Implementation (OSDI 18)*, pp. 595–610, Carlsbad, CA, October 2018. USENIX Association. ISBN 978-1-939133-08-3. URL <https://www.usenix.org/conference/osdi18/presentation/xiao>.
- Zhao, L. and Krishnamurthy, A. Bandwidth optimal pipeline schedule for collective communication, 2023.
- Zhao, L., Pal, S., Chugh, T., Wang, W., Basu, P., Khoury, J., and Krishnamurthy, A. Optimal direct-connect topologies for collective communications, 2022a.
- Zhao, Y., Liu, Y., Peng, Y., Zhu, Y., Liu, X., and Jin, X. Multi-resource interleaving for deep learning training. In *Proceedings of the ACM SIGCOMM 2022 Conference*, SIGCOMM '22, pp. 428–440, New York, NY, USA, 2022b. Association for Computing Machinery. ISBN 9781450394208. doi: 10.1145/3544216.3544224. URL <https://doi.org/10.1145/3544216.3544224>.
- Zheng, L., Li, Z., Zhang, H., Zhuang, Y., Chen, Z., Huang, Y., Wang, Y., Xu, Y., Zhuo, D., Xing, E. P., Gonzalez, J. E., and Stoica, I. Alpa: Automating inter- and Intra-Operator parallelism for distributed deep learning. In *16th USENIX Symposium on Operating Systems Design and Implementation (OSDI 22)*, pp. 559–578, Carlsbad, CA, July 2022. USENIX Association. ISBN 978-1-939133-28-1. URL <https://www.usenix.org/conference/osdi22/presentation/zheng-lianmin>.
- Zhu, Y., Eran, H., Firestone, D., Guo, C., Lipshteyn, M., Liron, Y., Padhye, J., Raindel, S., Yahia, M. H., and Zhang, M. Congestion control for large-scale rdma deployments. In *Proceedings of the 2015 ACM Conference on Special Interest Group on Data Communication*, SIGCOMM '15, pp. 523–536, New York, NY, USA, 2015. Association for Computing Machinery. ISBN 9781450335423. doi: 10.1145/2785956.2787484. URL <https://doi.org/10.1145/2785956.2787484>.

## A BANDWIDTH TIME OF ALLGATHER ALGORITHM FOR RAIL-OPTIMIZED AND RAIL-ONLY NETWORK

Zhao et al. (Zhao & Krishnamurthy, 2023) proved that a bandwidth-optimal AllGather schedule exists for arbitrary network topology. This section examines the best-case AllGather time for a grid of  $x \times y$  GPUs in the rail-optimized and rail-only network. Following Eq. 1 in Zhao et al. (Zhao & Krishnamurthy, 2023), we derive an analytical expression of the bandwidth AllGather time for these two types of networks.

Let  $\mathbb{M}_{xy}$  be the space of all boolean matrices of size  $x \times y$  except all ones and all zeros. A matrix  $A \in \mathbb{M}_{xy}$  represents a specific partition of the GPUs in an  $x \times y$  configuration. Then, the optimal AllGather time for one unit of data in a rail-optimized network is

$$\max_{A \in \mathbb{M}_{xy}} \frac{\max_{A' \in \{A, \bar{A}\}} \sum_{i,j} A'_{ij}}{\min_{A'' \in \{A, \bar{A}\}} ((C_F + C_S) \sum_{i,j} A''_{ij} - xR(A'')C_F)} \quad (8)$$

Here,  $\bar{A}$  denotes the negation of the boolean matrix  $A$ . The numerator finds the partition that sends the largest data, which equals the sum of the binary entries of  $A$  or  $\bar{A}$ . The denominator finds the partition with the lowest ingress and egress bandwidth. For each GPU included in the partition, the total bandwidth of the partition increases by  $C_F + C_S$ , hence the first term in the minimization. However, whenever the partition includes an entire row of GPUs (i.e., an HB domain), the bandwidth internal to this HB domain no longer contributes to the ingress or egress bandwidth. The function  $R(A)$  counts the number of rows with all ones as  $A$ 's entries, implying one HB domain entirely inside the partition. The second term in the minimization removes this part of the bandwidth from the egress bandwidth.

For the rail-only network, going through the same analysis, we get the AllGather time of

$$\max_{A \in \mathbb{M}_{xy}} \frac{\max_{A' \in \{A, \bar{A}\}} \sum_{i,j} A'_{ij}}{\min_{A'' \in \{A, \bar{A}\}} ((C_F + C_S) \sum_{i,j} A''_{ij} - xR(A'')C_F - yC(A'')C_S)} \quad (9)$$

The formula remains the same as Eq. 8, except for the last term in the denominator. This term accounts for the fact that whenever an entire rail is included in the partition, this rail no longer contributes its bandwidth as the ingress or egress bandwidth of the partition. Here, the  $C(A)$  function counts the number of columns with all ones as their entries, hence the number of entire rails inside the partition.

Intuitively, to maximize either expression, the choice of  $A$

Table 3. Extra parameters utilized in the appendix.

Name	Description
$N$	Total number of GPUs in the cluster
$M_{FF}$	Amount of feed-forward FLOPs required for an iteration
$M_{Attn}$	Amount of attention block FLOPs required for an iteration
$F$	GPU Compute Speed (FLOPs)
$B$	Global batch size
$R$	GPU memory size

should be skewed (i.e., having a large portion of GPU in one partition) so that  $\sum_{i,j} A'_{ij}$  on the numerator is large but  $\sum_{i,j} A''_{ij}$  on the denominator is small. In addition, the GPU choice should be arranged such that the denominator can exclude as much bandwidth from the partition as possible. For Eq. 8 and Eq. 9, one such configuration is obtained when the partition has  $y - 1$  HB domains. In this case,  $R(A'') = 1$  and  $C(A'') = 0$  which yield an AllGather time of  $(y - 1)/C_S$  per unit of data for both networks. We postulate that for  $C_F \gg C_S$  and  $x \geq y$ , this choice of partition yields the lower bound (thus bandwidth optimal) AllGather time for both of this network, as perturbing the partition by adding or removing single GPUs or entire HB domains only relaxes the bound. We leave concrete proof of the optimality in future work.

## B ESTIMATION OF MICROBATCH COMPUTE TIME

While LLM designers can use profiling to obtain microbatch computation times accurately, it is also possible to analytically estimate the execution time, especially when the hardware is unavailable. Table 3 shows the extra parameters used in this calculation and other sections in the appendix, in addition to Table 1.

Most FLOP for LLMs comes from the attention mechanism and general matrix multiplication (GEMM) in the feed-forward layers. Prior work reports that while GPUs operate at peak speed for GEMM in feed-forward layers, they are at most 40% efficient for attention blocks without architecture-specific optimization (Dao, 2023). Therefore, we model the computation time of a micro-batch accordingly, as

$$T_{\mu b}^{comp} = \frac{(M_{FF} + \gamma M_{Attn})b}{FBpt} \approx t(b) \quad (10)$$

where  $\gamma$  is a slowdown factor for attention. We use  $\gamma = 1/0.4$  for Section 6.  $M_{FF}$  and  $M_{Attn}$  depend on the model's hyperparameter and whether activation recomputation is utilized. Our evaluation in Section 6 assumes the training uses selective activation recomputation presented by Korthikanti et al. (Korthikanti et al., 2022), and the FLOPs estimation follows from Eq. 8 in the same paper.

## C CONSTRAINTS OF PARALLELIZATION CONFIGURATION

Given a cluster with  $N$  GPUs and an HB domain size of  $K$ , the following set of constraints hold for a valid parallelization strategy:

$$pdt = N \quad (11)$$

$$d_h t_h p_h = K \quad (12)$$

$$mb = \frac{B}{d} \quad (13)$$

$$d_l d_h = d \quad (14)$$

$$t_l t_h = t \quad (15)$$

$$p_l p_h = p \quad (16)$$

$$d_l, d_h, t_l, t_h, p_l, p_h, v, m, b \in \mathbb{Z}_{++} \quad (17)$$

$$\frac{l}{pv}, \frac{s}{t}, \frac{h}{t}, \frac{B}{d} \in \mathbb{Z}_{++} \quad (18)$$

$$\text{MemoryConsumption}(p, t, d) \leq R \quad (19)$$

In the constraints above,  $\mathbb{Z}_{++}$  refers to all positive integers. The first two constraints are guarantees that the parallelization strategy uses all physical GPUs in the cluster. Constraint 11 ensures that all GPUs in the cluster participate in the training. Constraint 12 ensures that the total parallelization dimensions map to the HB domain covers the entire domain.

Then, Constraint 13 establishes the relation of micro-batch size, number of micro-batches, and local batch size.

Constraint 14 to 18 ensures that the mapping from the parallelization strategy to the physical cluster is valid. Constraint 14 to 16 divides each of the parallelization dimension into grids of GPUs that spans HB and network domains. Constraints 17 guarantees that each parallelization dimension, interleaving size, micro-batch size, and micro-batch counts are integers in the final solution. In the end, Constraints 18 requires the ratio of a few parameters also to be integers.  $\frac{l}{pv}$  is the number of transformer blocks per interleaved scheduling stage.  $\frac{s}{t}$  and  $\frac{h}{t}$  refers to the number of sequences and hidden dimensions each GPU gets when  $t$ -way tensor (and sequence) parallelism is applied. Finally, the local batch size is  $\frac{B}{d}$ .

Finally, Constraint 19 ensures that LLMs parallelized with the generated parallelization strategy fit in the GPU RAM. We follow Korthikanti et al. (Korthikanti et al., 2022) for calculating the memory consumption of the LLM with selective activation recomputation.

We exhaustively generate all valid configurations for a given GPT model and the network cluster in the evaluation. While the nature of minimizing Eq. 2 subject to all constraints in this section is non-convex, there are a limited number of valid configurations. For instance, the GPT-1T with 128

GH200 computers yielded  $O(10000)$  possible configurations, making an exhaustive search possible.

## D RAIL-ONLY NETWORK SLOWDOWN FOR ALL-TO-ALL TRAFFIC

This section computes the slowdown of All-to-All traffic in a rail-only network compared to a rail-optimized network. We utilize the hierarchical All-to-All algorithm described in DeepSpeed Zero++ (Microsoft, 2023) for the rail-only network, but the result remains the same for a straightforward two-hop forwarding scheme.

Consider a grid of  $x \times y$  GPUs where each  $x$  lives in an HB domain, and the  $y$  HB domains are connected with a slower network domain. For All-to-All traffic in a rail-optimized network, every GPU sends to all other GPUs within an HB domain through the local fast interconnect and sends the rest of the traffic directly to their destinations through the full-bisection network. Assuming each shard to send is of size  $D$ , the total completion time is:

$$\begin{aligned} T_{a2a}^{Full\ Bisec} &= \max\left(\frac{(x-1)D}{C_F}, \frac{x(y-1)D}{C_S}\right) \\ &= \frac{x(y-1)D}{C_S} \end{aligned} \quad (20)$$

The hierarchical algorithm runs an All-to-All locally for the rail-only network that prepares each GPU to have all data to send on its rail. In this step, the effective data shard size is  $xD$ . Then, within each rail, the GPU runs a second All-to-All to finalize the algorithm with an effective shard size of  $xD$ . The total transmission time is

$$T_{a2a}^{Rail\ Only} = \frac{y(x-1)D}{C_F} + \frac{x(y-1)D}{C_S} \quad (21)$$

Note the two terms differ by  $y(x-1)D/C_F$ , which is the cost of forwarding All-to-All traffic within HB domains. When  $y(x-1) \approx x(y-1)$ , the slow down factor is approximately

$$\frac{T_{a2a}^{Rail\ Only} - T_{a2a}^{Full\ Bisec}}{T_{a2a}^{Full\ Bisec}} \approx \frac{C_F}{C_S} \quad (22)$$



Table 4. Model hyperparameters and iteration time comparison.

Model Size	Attention Heads	Hidden Size	Layers	TP Size	PP Size	Number of GPUs	Global Batch Size	Micro-batch Size	Number of Interleaved Stages	Measured Iteration Time in (Korthikanti et al., 2022)	Computed Iteration Time from Section 5
22B	64	6144	48	8	1	8	4	4	1	1.10	0.78
175B	96	12288	96	8	8	64	64	1	3	13.75	11.89
530B	128	20480	105	8	35	280	280	1	3	37.83	35.29
530B	128	20480	105	8	35	2240	2240	1	3	39.15	35.56
1T	160	25600	128	8	64	512	512	1	1	71.49	70.69

## E DETAILS OF MODEL HYPERPARAMETERS IN SECTION 6

Table 4 presents the detailed parameters for the LLM models evaluated in Section 6. We utilize the same batch size, micro-batch size, parallelization strategy, schedule interleaving, and enabled selective activation computation, as in Korthikanti et al. (Korthikanti et al., 2022), to obtain the result in Figure 8. Although Narayanan (Narayanan et al., 2021) et al. also present a similar evaluation in MegatronLM, the paper did not report the exact micro-batch size and interleaving count. Therefore, we cannot get an accurate estimation to compare for our formulation. The analysis in Section 4 is unaffected by the micro-batch size and assumes no interleaving, and adding interleaving does not change the analysis result.